CHEMISTRY OF MATERIALS

pubs.acs.org/cm

Article

Polyethylene Glycol-Mediated Switchable Blue-Green Emissions in Sulfur Nanostructures Controlled through the Surface Chemistry

Junkai Ren, Luca Malfatti, Luigi Stagi, Davide Carboni, Roberto Anedda, Laura Calvillo, and Plinio Innocenzi*

Cite This: *Chem. Mater.* 2022, 34, 8456−8468

Read Online

ACCESS | Metrics & More | Article Recommendations | Supporting Information

ABSTRACT: Metal-free sulfur nanodots are an emerging class of nanoparticles for applications in photonics and nanobiotechnology. Because of the stable photoluminescence (PL) and low toxicity, pure elemental quantum dots, such as S-dots, are excellent candidates for a new generation of 0D nanomaterials. However, they require a proper design to control the PL and obtain an excitation-independent emission. Here, we show that the control of the S nanostructure emission can be achieved by modulating the surface interface with an organic polymer, polyethylene glycol (PEG-400), which is widely used to passivate the nanostructure surface. Blue and green emissions can be switched on or off through PEG-400. The fluorescent S nanomaterials have been synthesized by thermally treating S powders in an alkaline solution and adding controlled amounts of PEG-400. The polymer triggers the formation of organosulfur compounds, with a remarkable modification of the characteristic emission of the S products. The sample emission shifts from blue to green by controlling the polymer concentration in the solution. The intensities of the two emissions can be tuned by adjusting the amount of PEG that favors the surface oxidation of the S nanostructure. A lower degree of oxidation causes an emission in the blue range, and higher oxidation of the sulfur atoms promotes an emission to the green.

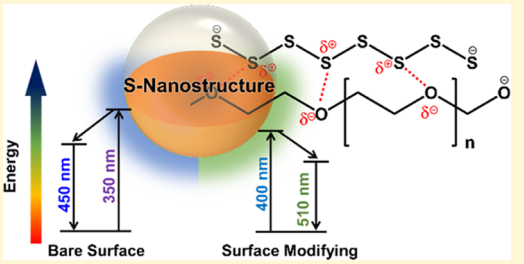

INTRODUCTION

New families of fluorescent 0D nanomaterials are emerging as feasible alternatives to conventional metal and rare-earth-based semiconductors.[1] Among them, colloidal heavy metal-free quantum dots, such as carbon, silicon, and phosphorus, are the best-performing nanomaterials because of their low toxicity, optical stability, tunable photoluminescence (PL), and high brightness.[2−4] The outstanding properties that arise from the combined effects of size, edge, core, and surface states have further stimulated the development of novel optical nanomaterials to extend their application fields.[5−7]

The properties of dots made by single-element sulfur (S), an inexpensive and abundant element, have also been used in lighting. Despite the difficulties in fabricating sulfur quantum dots (S-dots) with high-quality and controlled luminescence, several researchers have successfully prepared different types of S-based nanomaterials. They have been tested as light-emitting diodes (LEDs), in photocatalysis, sensing, and bioimaging.[8−15] Fluorescent S-dots have been first prepared by etching Cd atoms from cadmium sulfide quantum dots. The S-dots have been applied as surface modifiers of titania for improving hydrogen production.[8] Another example is the synthesis of S-nanodots by reacting bulk S and alkali using surfactants as surface passivators. Such S-dots exhibit excitation-dependent emissions in the green-to-blue region as a function of the reaction time.[9] S-dots have been also obtained via a bottom-up route using sodium thiosulfate as raw material and have been used to discriminate multiple metal ions.[10]

Different models to explain the fluorescence origin of S-based nanomaterials have been proposed.[16,17] Size dependence has been considered the main reason for the emission shift. An inhomogeneous size distribution produces the excitation-dependent fluorescence due to the quantum size effect.[9,11,14] Most of the S-dots synthesized so far present a broad distribution in size, and precise control of the emission has not been yet achieved. Obtaining a high PL efficiency is mandatory to fulfil the strict requirements to apply the S nanomaterials in optoelectronics and nanobiology. The use of hydrogen peroxide to etch the resulting S-dots allows for controlling their size and a fine-tuning of the emissions; the passivation-assisted elimination of surface traps enables an improved quantum yield (QY) up 23%.[11] The preparation of nanodots via the same method, but in an oxygen atmosphere, accelerates the process; S-dots with a nearly monodisperse size and QY of 21.5% have been obtained.[12]

Received: July 27, 2022
Revised: August 29, 2022
Published: September 9, 2022

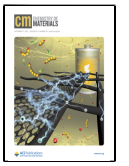

Although important achievements have been made, the development of phosphors based on sulfur is still in an initial stage, both from the applied and basic science point of view.[16,17] Fluorescent S-dots that combine controlled emission with a simple and reproducible synthesis are still challenging to produce. Furthermore, a complete understanding of the chemistry of this type of nanodots is far from being achieved. On the other hand, the origin of the emission is still not clear, in particular, the role of the surface states in regulating the fluorescence. In this context, the so-called "passivating agent," typically a polymer used to stabilize the nanodot surface and preserve the nanoparticles from aggregation in solution, plays a major role. Although several articles have been published in the scientific literature on the synthesis of S-dots, the origin of their fluorescence is still ambiguous. The results published so far indicate the sulfur crystalline core as the origin of the main emission, while the surface states modulate the fluorescence wavelength. However, it has not yet been possible to explain the chemical−physical process underlying it in more detail. The most common synthesis uses a polymer, PEG-400, as a stabilizing agent, but its effect on the nanodot emissions is poorly understood. In this work, we studied how to control the emission through the dot surface design to obtain a precise surface state—emission correlation. The controlled passivation of the S nanostructures by PEG-400, which forms a chemical bond with S, allows for modulating the emission from blue to green.

RESULTS AND DISCUSSION

The S nanostructures have been prepared by sequential steps, from the dissolution of the precursor S source in an alkaline environment to the purification to obtain samples of controlled dimension (Scheme 1). We have experimentally observed that

Scheme 1. Schematic Illustration of the Synthesis of PEG-Modified S Nanostructures

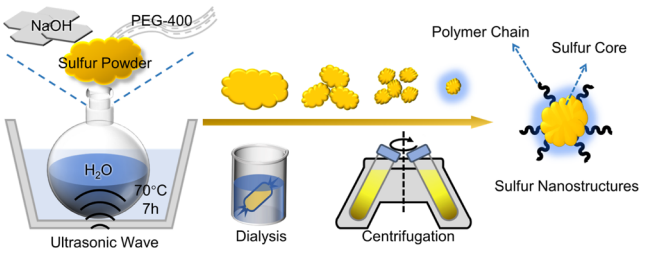

the synthesis can be easily achieved by combining sonication with heating. The simultaneous treatments promote the dissolution and dispersion of the sulfur powders in the alkaline solution (see Figure S1). The addition of different amounts of PEG-400 in the precursor solution allows for controlling the passivation of the S nanostructure surface. At the end of the purification process, S-based products of nanometric size and passivated by PEG-400 have been obtained. It should be observed that previous reports about the synthesis of S-nanodots mostly describe the use of PEG-400 as a dispersing agent to avoid agglomeration of the nanoparticles.[18] The formation of a chemical bond between the polymer and the S nanosurface has never been noticed or reported.

Optical Properties. Figure 1 shows the 3D excitation (y)—emission (x)—intensity (normalized intensity false color scale) fluorescence spectra, of S-based nanostructures passivated with different amounts of PEG-400 (0, 1.5, 3.0, and 4.5 g). The fluorescence of S nanostructure changes as a function of PEG-400 employed in the synthesis. Bare S samples without PEG-400 modification (0 g) have a well-defined excitation-independent blue fluorescence with a weak contribution in the green range (Figure 1a).

The addition of an intermediate amount of PEG-400 (1.5 or 3 g) enhances the second emission in the green (Figure 1b,c). A two-color emission, blue and green, is observed in these samples even if the blue emission is still the highest intensity component. In the 3 g of the PEG S-nanostructure, the two emissions are both intense and well-identified (Figure 1c). The blue emission maximum is at 450 nm upon excitation in the 300−400 nm range. The green emission is, instead, centered at 510 nm when the sample is excited between 380 and 450 nm. The fluorescence maps show a direct dependence of the emission of the sulfur nanostructures on the amount of the polymer used in the synthesis. The PEG-400 modulates the emission according to its concentration, shifting it from blue to green, and a two-color emission can be achieved by properly tuning the amount of the polymer. In the synthesis that employs the highest amount of PEG-400 (4.5 g), the blue emission component is very weak while the green one becomes predominant over the whole spectrum (Figure 1d).

The rise of a green emission that increases with the amount of PEG-400 would suggest that the polymer is the source of such fluorescence shifts. We also synthesized samples starting from PEG-400 alone to verify this hypothesis under the same conditions used to prepare the S nanostructure. The samples obtained from the PEG-400 are, however, emitting only in the blue region. In addition, they show an excitation-dependent emission in the 350−600 nm range with a maximum at 430 nm (Figure S2). The different emission properties of PEG and PEG-modified S samples indicate that the green fluorescence does not originate from the byproducts of PEG-400 but rather from a different distribution of the surface state on the samples affected by the presence of PEG-400. In general, the shift of fluorescence in the S nanostructure is attributed to a size effect.[9,11,14] According to this interpretation, the emission maxima shift to shorter wavelengths with the decrease in the particle size. Furthermore, most of the S-dots reported in the scientific literature exhibit excitation-dependent emission, which has been mainly assigned to their inhomogeneous size distribution.[9,14] A size-dependent fluorescence model does not explain the present experimental results; the resulting S nanostructures, in fact, do not exhibit two well-defined size-ranges that could explain the switchable bi-luminescence (vide infra).

Figure 2a shows the absorption spectra in the 250−500 nm range of the four S-based samples (the corresponding UV−vis full spectra are reported in Figure S3); the curves have been deconvoluted by Gaussian functions to identify the different components. A good fit has been obtained using four absorption curves, two in the UV and two in the visible range.

The S nanostructures exhibit an intense deep UV band with a broad absorption tail that becomes more intense as a function of PEG-400 concentrations. The UV absorption has been deconvoluted using two components, indicated as UV I and UV II (pink and red curves in Figure 2a). The UV I, centered at ∼230 nm, is attributed to the $n \rightarrow \sigma^*$ transition of nonbonding electrons of S atoms. The UV II (red curve) is instead assigned to the polysulfide S^{2-} species on the surface of S nanostructures. The attribution of this band has been carried out using the work of Manan et al. as a reference, who

https://doi.org/10.1021/acs.chemmater.2c02284
Chem. Mater. 2022, 34, 8456−8468

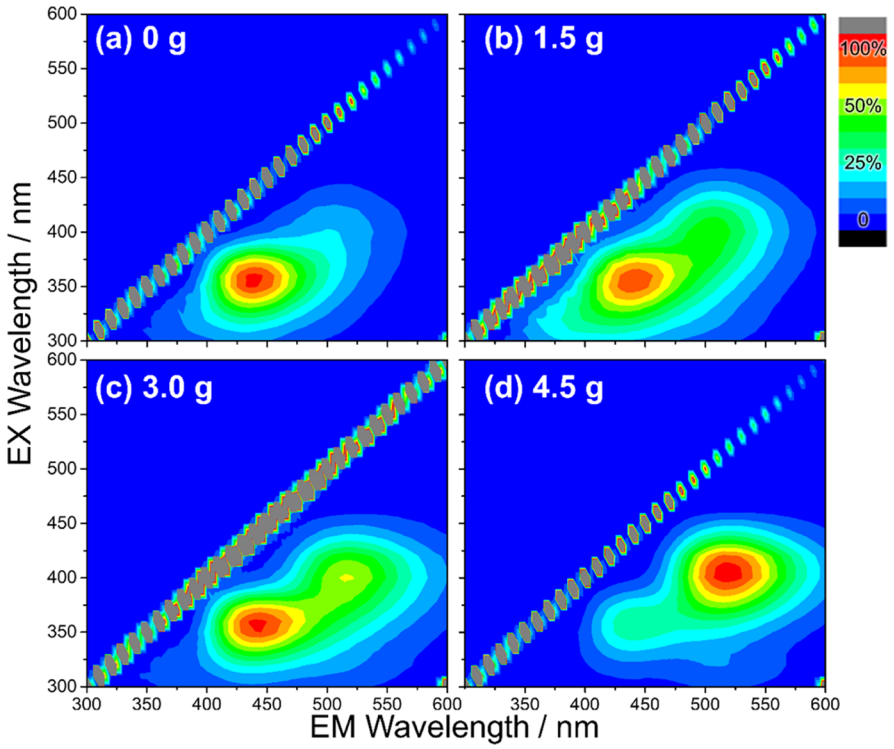

Figure 1. 3D PL excitation (*y*-axis)—emission (*x*-axis)—intensity (normalized false color scale) spectra in the 300−600 nm range: (a) bare S (0 g); (b) PEG-modified S (1.5 g); (c) PEG-modified S (3.0 g); and (d) PEG-modified S (4.5 g) nanostructures. The amount in grams corresponds to the PEG-400 used in the synthesis. The diagonal gray lines are generated by the first order of excitation light.

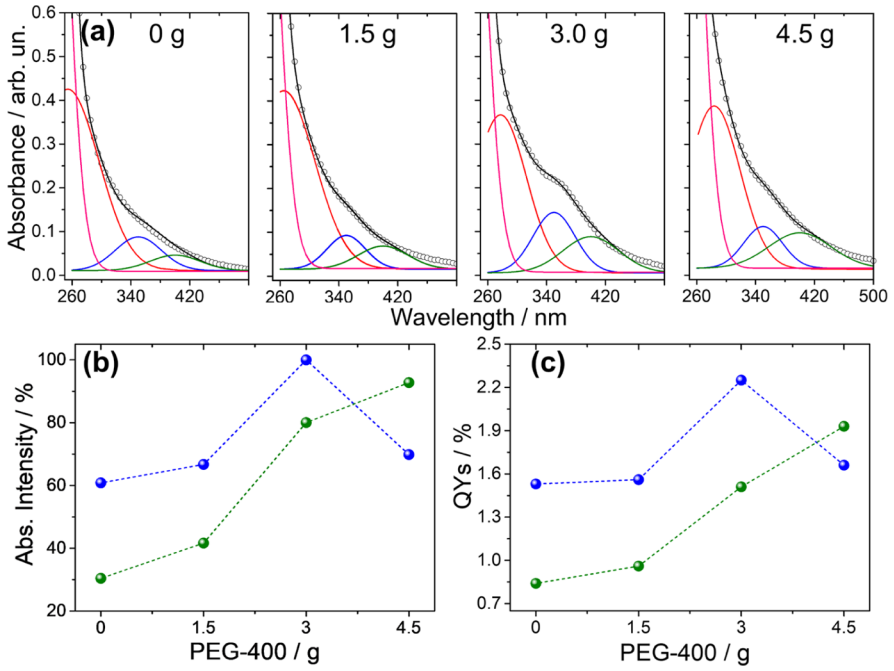

Figure 2. (a) UV−vis absorption spectra and corresponding Gaussian fitting in the 250−500 nm range from different S-nanostructures. The hollow dots represent the experimental results; the black line is the Gaussian fit. The different Gaussian components are indicated with pink (UV I), red (UV II), blue (λ = 350 nm), and green lines (λ = 400 nm). (b) Relative absorption intensities of the bands at 350 (blue dots) and 400 nm (green dots), as a function of the amount of PEG-400 added for the synthesis. The dot lines are a guide for the eyes. (c) QYs of the S dots excited at 350 (blue dots) and 400 nm (green dots), as a function of the amount of PEG-400 added for the synthesis. The dot lines are a guide for the eyes.

correlated the different S species observed by voltammetry in non-chloroaluminate ionic liquids with the UV−vis spectra.[19]

In the visible region, a broad tail that ends in the green wavelengths characterizes the absorption spectra. Previous studies have overlooked this specific conformation of the absorption curve, but it contains important information if adequately analyzed. It is composed of at least two components, one in the blue and the other one in the green.

https://doi.org/10.1021/acs.chemmater.2c02284
Chem. Mater. 2022, 34, 8456−8468

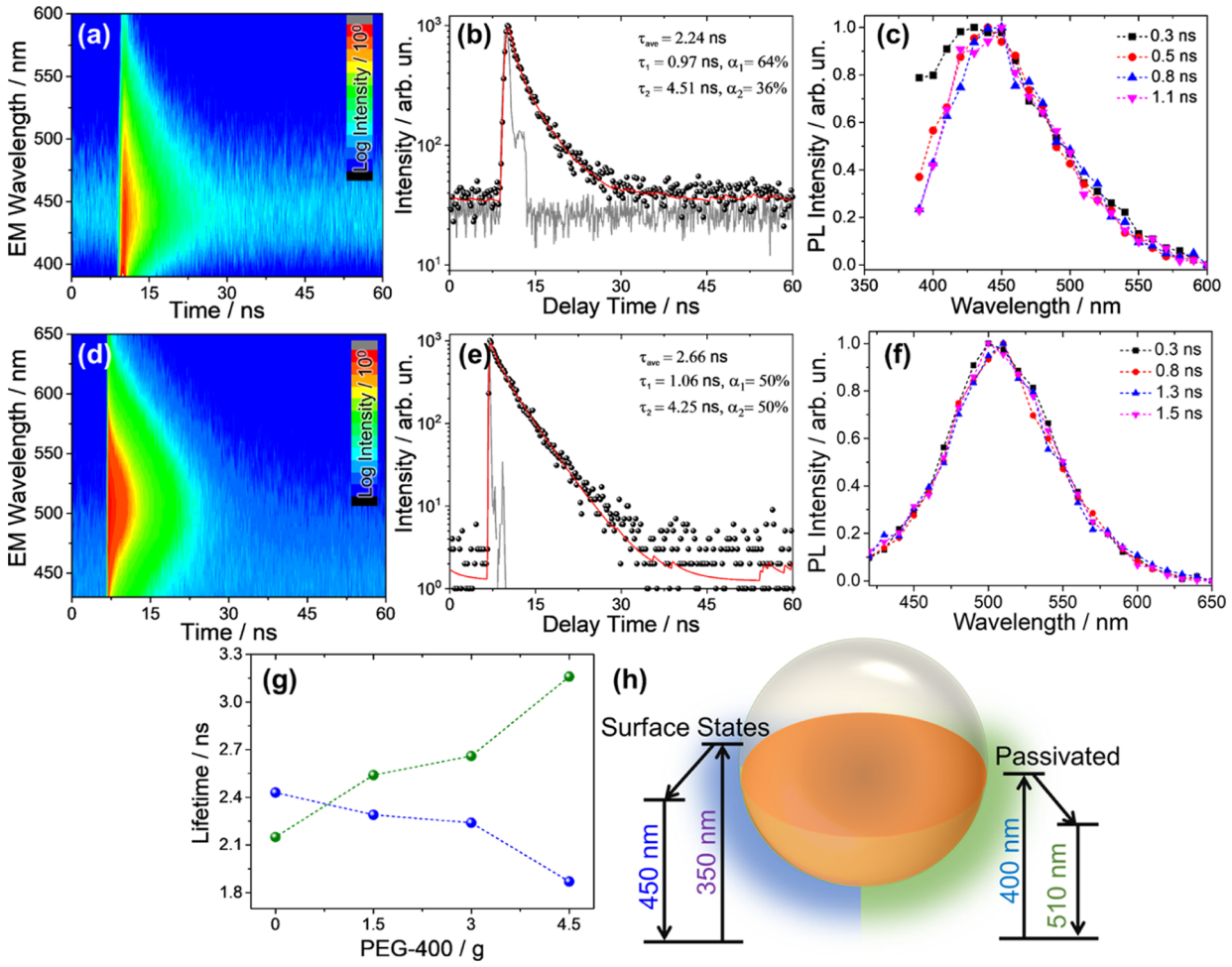

Figure 3. (a) TRES maps of the S-nanostructure (3.0 g) λ_{ex} = 350; *x* and *y*-axis are the time and emission wavelength, respectively. The colors from blue to red indicate the logarithmic emission intensity change from low to high. (b) Emissive decay curves with the fitting results, λ_{em} = 400 nm, λ_{ex} = 350; the fit is the red line, and the dots are the experimental data. (c) Normalized emission spectra extracted from the streak image at different decay times, λ_{ex} = 350. (d) TRES maps of the S-nanostructure (3.0 g) λ_{ex} = 400 nm. (e). Emissive decay curves with the fitting results, λ_{em} = 510 nm and λ_{ex} = 400; the fit is the red line, and the dots are the experimental data. (f) Normalized emission spectra extracted from the streak image at different decay times, λ_{ex} = 400. (g) Average lifetime of emissions at 450 (blue dots) and 510 nm (green dots), respectively, as a function of the amount of PEG-400 added for the synthesis. The dot lines are a guide for the eyes.

Using the same method applied to identify the UV II band, they are assigned to S_4^{2-} and SO_3^{2-} species. The two bands are exactly correlated to the excitation wavelengths of the blue and green emission maxima (Figure 1). The plots in Figure 2b,c show the change in intensity of the absorption bands peaking at 350 and 400 nm and the corresponding QYs at these two wavelengths (see Figure S4 and Table S1). The absorption and QY curves are well correlated. The blue component increases in intensity and QY with the PEG-400 but suddenly drops when the highest amount of the polymer is employed. The green component, instead, shows a continuous increase in absorbance and QY with the polymer amount.

Time-resolved fluorescence can provide further insights into the luminescence mechanism of optical materials. Time-resolved emission spectra (TRES) are a sequence of PL lifetime data recorded at increasing PL wavelengths, which give the signature of the emission shift as a function of the fluorescence timescale. The TRES maps of the four samples have been acquired by time-correlated single-photon counting using the excitation wavelengths at 340 (Figure 3a) and 400 nm (Figure 3d) (the whole spectra are shown in Figure S5).

Taking the PEG-S-nanostructure (3.0 g) as an example, the PL decay curve at 450 nm (λ_{ex} = 340 nm) can be fitted by a bi-exponential function (Figure 3b); the average value is 2.24 ns, which is between the shorter (0.97 ns, 64%) and the longer (4.51 ns, 36%) values. Figure 3c shows that the blue emission does not shift with the time after the excitation pulse, which means that only a single type of blue emissive center in the prepared S-nanostructure exists.[20,21]

Figure 3d shows the TRES map of the 3 g of the sample with λ_{ex} = 400 nm. The average value calculated taking the decay curve at 450 nm is 2.66 ns with two recombination lifetimes, 1.06 and 4.25 ns (Figure 3e). Moreover, in the case of the green emission, no shift with the change in decay time is observed, indicating that only one emissive center accounts for the green light (Figure 3f).

Figure 3g shows the change in the average lifetimes of the blue and green components of the S-nanostructures as a function of the PEG-400 amount; Table S2 summarizes the fitted results of the relative TRES data. The blue emission lifetime decreases while the green one increases with PEG-400, which agrees well with the transition from blue to the green of the luminescence. Interestingly, the lifetime of the green

https://doi.org/10.1021/acs.chemmater.2c02284
Chem. Mater. 2022, 34, 8456−8468

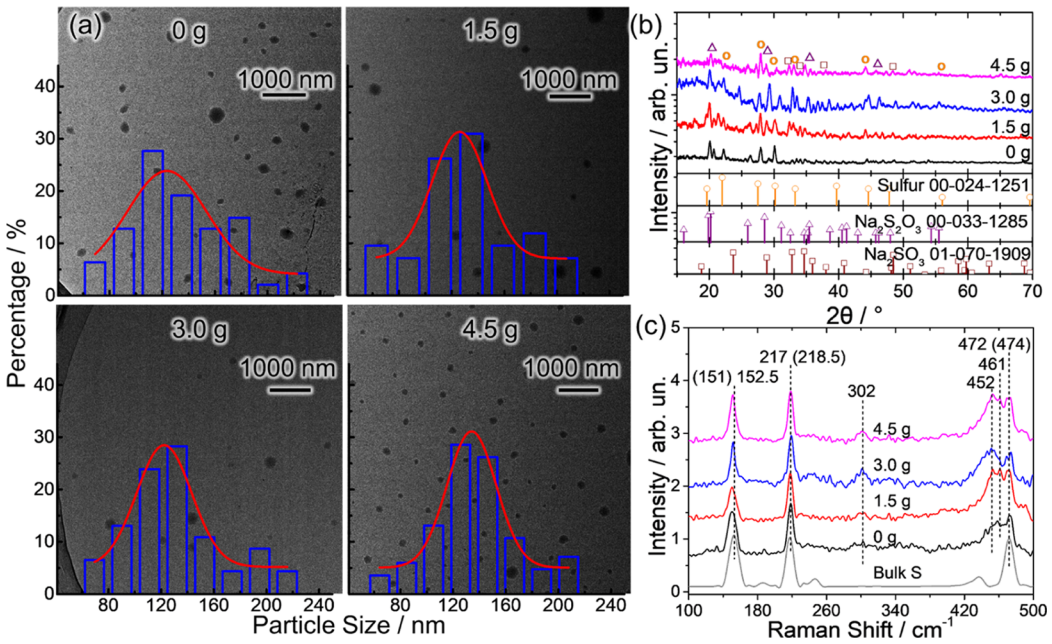

Figure 4. (a) TEM images (the overlapped pictures show the size distribution histograms), (b) XRD patterns (the marks at the bottom are the diffraction peaks of sulfur, $Na_2S_2O_3$, and Na_2SO_3), and (c) Raman spectra of different S nanostructures. The gram values (0−4.5 g) represent the amount of PEG-400 added for the synthesis.

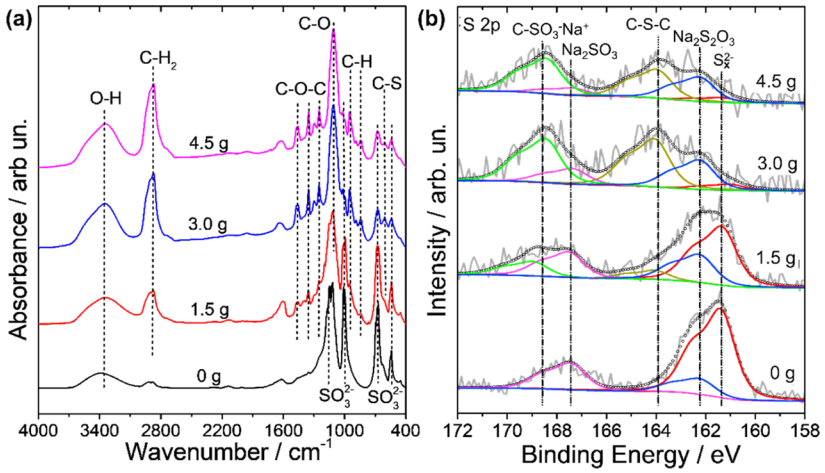

Figure 5. (a) FTIR absorption spectra and (b) high-resolution XPS spectra for S 2p of different S nanostructures prepared using 0, 1.5, 3, and 4.5 g of PEG-400.

emission is longer than that of the blue light. The two-color emissions can be explained by assuming an S-structure surface modification induced by the PEG. We hypothesize that the polymer can modify the nanostructures' oxidation state at the surface and facilitates the radiative pathways that lead to emission at lower energies in the green region (Figure 3h).

Morphology and Composition. To figure out the formation of the S-nanostructures, we have extensively investigated the structural and chemical properties of the nanoparticles. The transmission electron microscopy (TEM) images in Figure 4a reveal that the four samples have spheroidal structures with an average size of 120 ± 10 nm, which is larger than other reports (nanodots, usually in the 5−20 nm range).[11,12,22] It should be underlined that the presence of PEG-400 does not change the size and distribution of the S-based samples that is in the ∼60−220 nm range, and, most importantly, does not lead to the so-called excitation-dependent emission. However, if the fluorescence source is the crystalline core of the S-structure that is responsible for the quantum confinement of the electrons, a size-dependent emission must be observed.

Interestingly, the introduction of the polymer narrows down the size distribution of the nanoparticles: the full width at half-maximum (fwhm) of the Gaussian fitting curves is reduced from 71 to 44 nm. Unfortunately, the low electronic contrast between the S products and the carbon-coated copper grid does not allow a precise determination of the edges or the crystallite structure.

X-ray diffraction (XRD) analysis in Figure 4b shows that complex diffraction patterns in the 10−70° 2θ range characterize the four S-nanostructures. The patterns are indexed as sulfur (S), sodium sulfite (Na_2SO_3), and sodium thiosulfate ($Na_2S_2O_3$). Herein, we cannot simply attribute the diffraction pattern to a single orthorhombic S8 or hexagonal S6

https://doi.org/10.1021/acs.chemmater.2c02284
Chem. Mater. 2022, 34, 8456−8468

phase.[9,23] According to the ICDD database (no. 00-024-1251), the crystalline phases of our S nanostructure have different compositions that result from the reaction pathway, as also supported by Raman analysis (vide infra).

Figure 4c shows the Raman spectra of the S samples. The bands at 152.5, 217, and 472 cm^{-1} are assigned to S−S bending and stretching modes in bulk sublimed S powder.[24] They shift to 151, 218, and 474 cm^{-1} in the four S-nanostructure particles. Although no differences between S nanomaterials and their raw S powder are generally reported in the analysis by Raman spectroscopy,[9,12] the slight blue and red shifts have to be considered. The changes in the Raman spectra suggest that the resulting S-based samples have a complex composition with the presence of different phases.[24] The addition of PEG-400 to the synthesis correlates with the appearance of three Raman bands, the first peaked at 302 nm, and the others partially overlapped at 452 and 461 cm^{-1}. The mode at 302 cm^{-1} is assigned to the deformation of C−S−C while those at 452 and 461 cm^{-1} to the stretching, $\nu_{(S-S)}$, and deformation, $\delta_{asym(O-S-O)}$, of thiosulfate.[25] Interestingly, the appearance of the 302 cm^{-1} band suggests the formation of thioethers (C−S−C) through a chemical reaction between the PEG and the S structure.[26]

Fourier-transform infrared (FTIR) spectroscopy analysis (Figure 5a) of the four samples has also been used to verify the formation of S particles during the reaction. The bare S-nanostructures prepared are characterized by vibrational modes at 1110, 1001, 673, and 540 cm^{-1} attributed to sulfite.[27] Apparently, increasing amounts of PEG-400 in the synthesis cause a decrease in intensity of the infrared bands assigned to sulfite. Although this hypothesis cannot be ruled out, the change in the relative S-nanostructure/PEG-400 weight ratio in the different samples could be the origin of the effect. Interestingly, another absorption band at smaller wavenumbers, 610 cm^{-1}, also shows a correlation with the amount of PEG-400 in the sample. Considering the trend, this band cannot be attributed to the polymer or sulfur-based compounds formed in the bare S-nanostructure. We attribute this band to the C−S stretching of organosulfur species (thiolates and thioethers) formed from the reaction between the organic polymer and the sulfur on the nanostructure surface.[26] The presence of PEG-400 on the particle surface is revealed by the absorption bands at 2878, 1350, and 1105 cm^{-1}, assigned to C−H_2, C−O−C, and C−O vibrational modes, respectively.[28] The successful passivation of the S nanostructures by the PEG chain (see Figure S6) can be monitored by observing the trend of the C−H_2 bending mode at 2878 cm^{-1}. Although both sulfate and thiosulfate show weak bands in the same range (Figure 5a, black line), the intensity of the 2878 cm^{-1} band linearly increases with the PEG amount, indicating a chemical interaction of the polymer at the dot surface. In the 750−500 cm^{-1} infrared region (Figure S7), two overlapped bands of small intensity are detected at 626 and 610 cm^{-1}. In the bare S-samples, the 610 cm^{-1} band is not detected while it increases in intensity with the increase in PEG-400 in the samples. The ratio between the intensity measured at 610 cm^{-1} with respect to the maximum of the C−H_2 band (2871 cm^{-1}) increases from 0.791 to 0.807 in the samples prepared with 3.0 and 4.5 g of PEG-400, respectively.

The wide and intense band at 3370 cm^{-1} is assigned to the absorbed water, the hydroxyl groups on the dot surface, and the terminal −OH of the PEG-400.[29,30] Two overlapping components peaking at 3280 and 3340 cm^{-1} have been resolved through Gaussian deconvolutions (Figure S8); the bands increase in intensity after modification with more PEG-400. The O−H content on the surface of S nanostructures rises from 12 to 60% (bare S sample vs PEG-modified S sample), indicating an enhanced functionalization and an improved dispersibility in the solvent. The corresponding O−H stretching overtone in water also increases from 25 to 45% because the polymer chains can allow adsorbing more water molecules.

X-ray photoelectron spectroscopy (XPS) has been employed to identify the chemical composition and chemical state of the S nanomaterials as a function of the PEG-400 amount. The XPS survey spectra (Figure S9) show that the sample surfaces are composed of O, Na (Auger peak at around 497 eV), C, and S. Although the presence of Na in previous studies has been mostly ignored,[13,14,31] the Na element is an important component in the resulting S nanostructures. Na plays an important role to stabilize the existing sulfite and thiosulfate species as salts.

The high-resolution XPS S 2p spectra of bare S nanostructure (see Figure 5b) can be deconvoluted into four doublets originating from $2p_{3/2}$ and $2p_{1/2}$ with a spin−orbit splitting of ∼1.18 eV. The percentage variation of the four components is resumed in Table S3 of Supporting Information. The sample prepared with no PEG shows an XPS spectrum composed of two main $2p_{3/2}$ peaks, located at 161.4 and 167.4 eV, which can be assigned to S_x^{2-} (sulfide, 66.1%) and SO_3^{2-} (sulfite, 20.8%).[32,33] Meanwhile, we also observe a peak at 162.2 eV that is associated with the formation of a third sulfur-based compound, thiosulfate ($Na_2S_2O_3$), in agreement with the XRD findings. As soon as the PEG concentration increases, the intensity of thiosulfate expands from 13.1 to 24.3%, while the component associated with sulfite progressively disappears. In addition, when PEG is added to the dot synthesis, two new components, centered at 164.0 and 168.4 eV, appear. The former is attributed to the formation of thioether bonds C−S−C while the latter to the sulfonate (C−SO_3−Na^+).[34] These components increase with the PEG contents, suggesting the formation of a chemical bond between polymer fragments and the sulfur atoms at the sample surface. It is also worth noting that the component at 164.0 eV could also be assigned to the presence of bulk sulfur; however, this attribution can be discharged considering that the component increases with the amount of PEG. The formation of the C−S−C bond,[35] as indicated by the XPS binding energy band at 164 eV, is also supported by a new signal appearing at 168.8 eV in the PEG-modified S nanostructures. It corresponds to C−SO_3^-, which increases from 10.8 to 34.7% with the amount of PEG (see Table S3).[34] Finally, as can be seen from the survey spectra, the S 2p peak decreases as a function of PEG-400, suggesting that the dot surface is progressively coated by the polymer, reducing the S signals.

The experimental data allow giving a good description of the overall process. The formation of S-based nanostructures in strongly alkaline conditions has been previously described as a "dissolution-assembly-fission," which involves two reaction steps[9,11]

$$3S + 6NaOH \leftrightarrow 2Na_2S + Na_2SO_3 + 3H_2O \quad (1)$$

$$(x - 1)S + Na_2S \leftrightarrow Na_2S_x (x = 2 - 5) \quad (2)$$

The residual sodium cations remaining on the dot surface even after careful washing via dialysis explain the detection of

https://doi.org/10.1021/acs.chemmater.2c02284
Chem. Mater. 2022, 34, 8456−8468

Na_2S and Na_2SO_3 in the samples. Raman spectroscopy and XPS analyses of the samples prepared with an increasing amount of PEG-400 reveal the formation of a chemical bond between carbon and sulfur atoms. It is, therefore, reasonable to assume that, in strongly basic conditions, given the high nucleophilicity of the negatively charged species of sulfur, the resulting sulfides, such as Na_2S or S_x^{2-}, could react with the ether moieties of the PEG-400 to form thiolates as intermediate compounds as it follows

$$nNa_2S + -[OCH_2CH_2]_n - O^- \leftrightarrow 2nNa^+ + n(Na^+ - [OCH_2CH_2] - S^-Na^+) \quad (\text{exc. of } OH^-) \tag{3}$$

The progressive reaction of sulfide with PEG-400 fragments can also push the reaction toward the formation of thiosulfate (4), as observed by XPS in the sample with the PEG-400 content of 3 and 4.5 g

$$4S + 6NaOH \leftrightarrow 2Na_2S + Na_2S_2O_3 + 3H_2O \tag{4}$$

At the same time, the thiolate intermediate $-[OCH_2CH_2]-S^-$ species are expected to react forming both thioether compounds and sulfonates according to (5) and (6)

$$(-[OCH_2CH_2] - S^-)Na^+ + -[OCH_2CH_2]_n - O^- \leftrightarrow -[OCH_2CH_2] - S - [H_2CH_2CO]^- + NaS^- \tag{5}$$

$$H - [OCH_2CH_2] - S^- + Na_2SO_3 \leftrightarrow H - [OCH_2CH_2] - SO^{3-}Na^+ + NaS^- \tag{6}$$

Equations 3 and 5 are justified by considering the XPS trend where the component attributed at S_x^{2-} decreases while that of C−S−C increases as a function of the PEG-400 content. The sequence of reactions in (3) and (5) is graphically illustrated by the following Scheme 2.

Scheme 2. Proposed Mechanism for the Formation of Organosulfur Species during the Reaction between Sulfur and PEG-400 Fragments

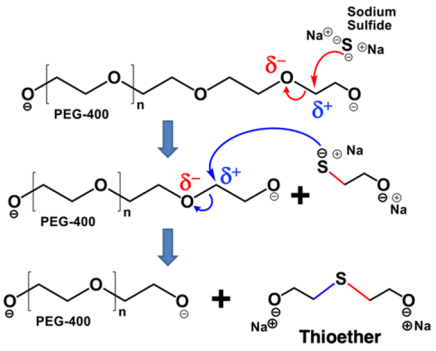

The use of PEG-400 during the dot synthesis favors the formation of a sulfur-compound with a higher degree of oxidation, such as thiosulfate, with respect to the naked S samples. This counter-intuitive concept can be understood considering the oxygen atoms in the ether moieties of the PEG-400 structure. They contribute to the S atom polarization at the bulk powder surface, promoting their oxidation processes and the consequent formation of thiosulfate sulfonates species (Scheme 3). The presence of thiosulfate on the dot surface, in turn, empowers the emission in the green range, enabling the two-color emission switch.

Scheme 3. Polarization of the Sulfur Atoms Operated by the Oxygen Atoms Present onto the Ether Moieties of the PEG-400 Structure

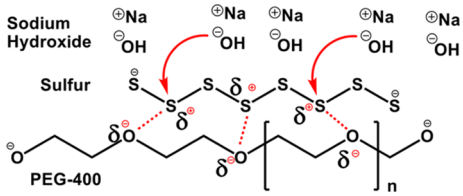

S-nanostructure synthesis has been performed in fully deuterated solvents (PEG-400 + sulfur + NaOD and D_2O) to confirm the mechanism, as described in Scheme 2. The reaction progress has been monitored through ^1H NMR by sampling small amounts of reaction mixtures after 1, 3, 7, and 13 h. A reference reaction has also been performed under the same conditions but using only PEG-400. The ethylene oxide backbone of the PEG gives the main ^1H NMR signal, which, from an overall integral evaluation, overwhelms the weakest signals by 15,000:1 (Figure S10). However, a detailed analysis of the ^1H NMR spectra has evidenced the rise of new signals not detected in the PEG-400. Figure 6 shows a small but clear

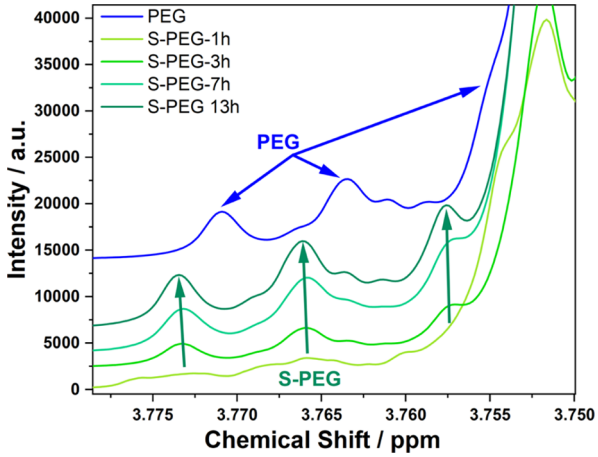

Figure 6. Detail of stacked ^1H NMR spectra showing a PEG triplet (top blue line) and the same triplet in the spectra of S-PEG after 1, 3, 7, and 13 h of the reaction (from bottom to top, as indicated by the arrow direction).

downshift of a triplet assigned to the PEG-400 ($-CH_2-O$, δ 3.76 ppm). This shift is due to the perturbation of the electron density of the C−O bond caused by the interaction with an electron-withdrawing species, most probably the negatively charged sulfur, as Scheme 3 shows.

The downshift effect slowly increases with the reaction time, supporting the hypothesis that the sulfur interacts with the carbon by perturbing the magnetic environment of the hydrogen of the methylene group and deshielding them. This effect weakens the C−O bond and makes the more electrophilic carbon prone to a nucleophilic attack. In addition to the above-described downshift effect, the reaction of PEG-400 with the sulfur produces new species, which, though in the low concentration compared to the bulk of PEG-400, support

https://doi.org/10.1021/acs.chemmater.2c02284
Chem. Mater. 2022, 34, 8456−8468

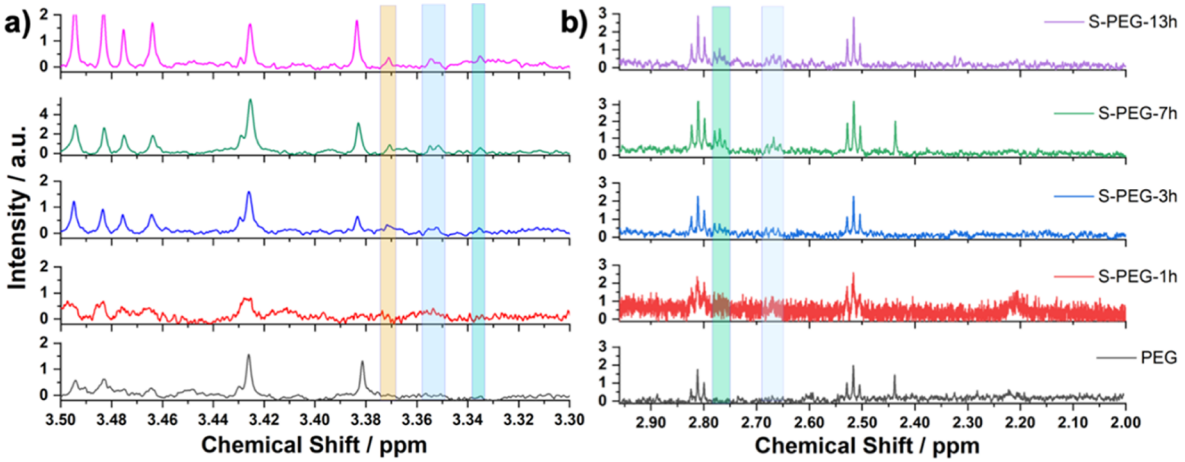

Figure 7. Detail of stacked ^{1}H NMR spectra showing the 3.50−3.30 ppm range (a) and the 3.0−2.0 ppm range (b).

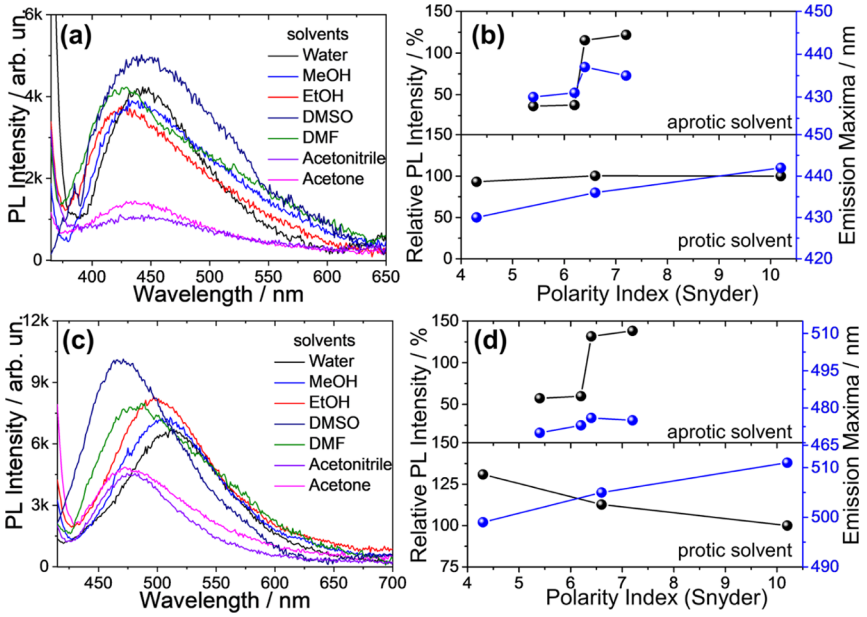

Figure 8. (a) PL spectra of bare S nanostructure (0 g) in different solvents under 350 nm excitation, (b) PL intensities (right *y*-axis, black dots) and emission maxima (left *y*-axis, blue dots) as a function of the solvent polarity index. The lines are a guide for the eyes. (c) PL spectra of the PEG-modified S nanostructure (4.5 g) in different solvents under 400 nm excitation, (d) PL intensities (right *y*-axis, black dots) and emission maxima (left *y*-axis, blue dots) as a function of the solvent polarity index. The lines are a guide for the eyes. The polarity indexes (Snyder) are 10.2 (water), 7.2 (dimethyl sulfoxide, DMSO), 6.6 (MeOH), 6.4 (*N*,*N*-dimethylformamide), 6.2 (acetonitrile), 5.4 (acetone), and 4.3 (EtOH) according to the ref 41.

the proposed mechanism. In particular, the ^{1}NMR spectra show two triplets (δ 2.78 and 2.68 ppm), a doublet (δ 3.35 ppm), and two singlets (δ 3.33 and 3.37 ppm) (see Figure 7).

The two triplets in Figure 7b have been attributed to organosulfur species containing methylene groups directly attached to the sulfur (i.e., CH_2-S-H). In contrast, the signal around δ 3.4 ppm (Figure 7a) has been assigned to the methylene groups in β with respect to the sulfur and in α to oxygen (i.e., $O-CH_2-CH_2-S-H$).[36] Alternatively, the latter could also be associated with methylene groups directly attached to sulfoxide groups derived from further oxidation of the original thiols ($-CH_2-S(O)_2-$).[37] These pieces of evidence justify the formation of organosulfur species through the mechanism described in eqs 3, 5, and 6 in Scheme 2.

Solvent and pH Effects. Physical−chemical changes in the nanodot environment, such as solvent polarity and pH, usually have significant effects on the emission properties of the fluorophores. Therefore, studying the responses of the S nanostructures to the changes in the chemical environment can give a better insight into the fluorescence origin. Figure 8 shows the fluorescence spectra of the nanostructures (0 g for blue emission and 4.5 g for green one) in different aprotic (acetonitrile and acetone) and protic solvents (water and ethanol). Both the blue and green emissions (in aprotic and protic solvents) are in good accordance with the Lippert-Mataga solvatochromic model.[38] The PL intensity in the protic solvent is weaker than that in the aprotic one because of the formation of stronger hydrogen bonding between fluorescent materials and their chemical environment.[39] In our case, the PL spectra of the S-based products in acetonitrile and acetone exhibit an abnormal decrease in intensity (40% for bare S samples and 60% for PEG-modified S samples; the data are

https://doi.org/10.1021/acs.chemmater.2c02284
Chem. Mater. 2022, 34, 8456−8468

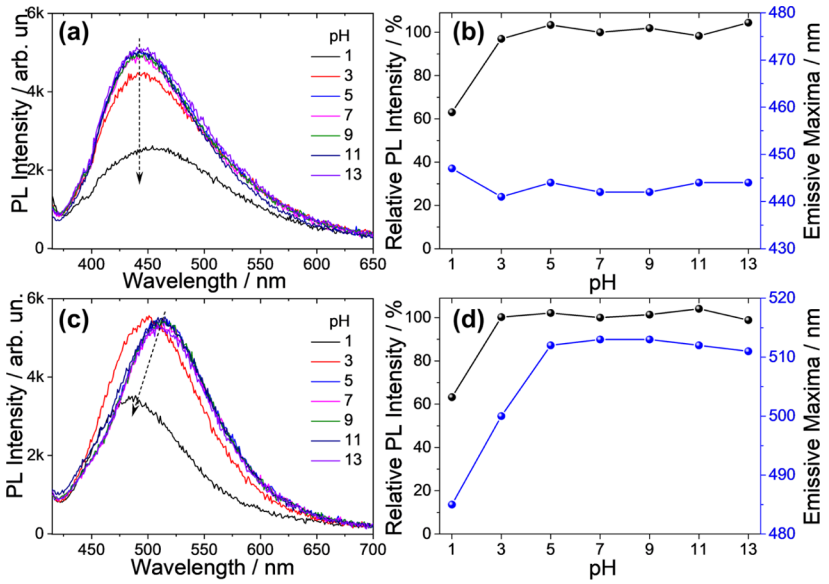

Figure 9. (a) PL spectra of bare S nanostructure (0 g) aqueous solutions at different pH values under 350 nm excitation, (b) PL intensities (right *y*-axis, black dots) and emission maxima (left *y*-axis, blue dots) as a function of pH. (c) PL spectra of PEG-modified S nanostructure (4.5 g) in solutions at different pH values under 400 nm excitation, and (d) PL intensities (right *y*-axis, black dots) and emission maxima (left *y*-axis, blue dots) as a function of pH.

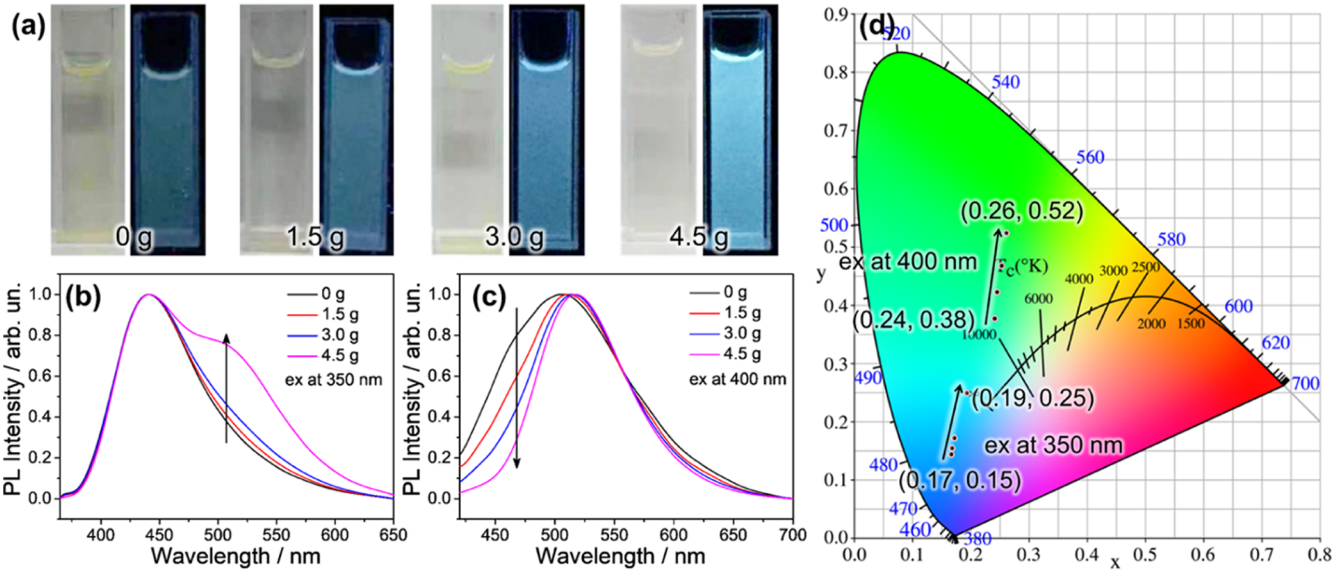

Figure 10. (a) Pictures of S-nanostructures in aqueous solution under sunlight (right) and UV light (365 nm, left). (b,c) Normalized PL spectra of S-nanostructures under excitation at 350 (b) and 400 (c) nm. (d) Chromaticity coordinates of the PL spectra of S-nanostructures in the CIE 1931 chromaticity diagram. The gram values (0−4.5 g) represent the amount of PEG-400 added for the synthesis.

normalized on the emission in water), which is caused by the relative poor dispersion in these media.

The solvatochromic changes are evident while observing the fluorescence of S nanostructures in protic solvents (see Figure 8d). The intensity decreases from 130 to 100%, while the emissive center shifts from 498 to 512 nm as the polarity increases from 4.3 to 10.2 (from EtOH to water). Notably, the green emission shows a clear red-shift when the aprotic solvents (470−475 nm) are replaced by protic ones (498−512 nm), which seems not to follow the linear relationship with the increase in the polarity index. This phenomenon is due to the formation of hydrogen bonding interactions via hydroxyl groups between the S nanosurface and the protic solvents.[40] In this case, the specific interactions, rather than the polarity index, are predominant for the green emission. The data support the origin of green luminescence from the surface states of the S nanoparticle. On the opposite, as shown in Figure 8b, the solvent effects are weaker for the bare S-nanostructure, indicating that the blue emissive center (band-to-band transitions) is not affected. The double emissions from the PEG-modified S-nanostructure (3.0 g) also present similar origins: as shown in Figure S11a,b, the blue emissive center shows a narrower solvation shift (424−440 nm) in different solvents. As shown in Figure S11c,d, the green fluorescence exhibits a broader emissive shift from 474 to 513 nm in the corresponding solvents.

Figure 9 shows the pH effects on the optical properties of the S-nanostructures (0 g for blue emission and 4.5 g for green

https://doi.org/10.1021/acs.chemmater.2c02284
Chem. Mater. 2022, 34, 8456−8468

one), which are recorded under different pH conditions of their aqueous dispersions. The two-color fluorescence response has been studied as a function of pH using the PEG-modified S nanostructures (3.0 g) (see Figure S12). Figure 9a shows the emission intensity changes of the blue component in the samples as a function of pH (from 1 to 13). The emission maxima are almost pH-independent but at pH 1, the intensity drops (Figure 9b). The green fluorescence is stable in the high pH range, 5−13, in terms of the emission wavelength and intensity but a blue-shift from 512 to 482 nm, and a dramatic drop in intensity is observed as pH decreases from 5 to 1 (Figure 9c,d).

These results suggest that the emission in the S nanostructures is affected by the chemical−physical environment, for example, solvent and pH, in agreement with the presence of emissive surface states.[42]

Figure 10a shows the pictures of S nanomaterial solutions under sunlight and UV light illumination. The color of samples changes from blue to green under UV irradiation as a function of the PEG-400 amount. The brightness also increases in accordance. The color change is caused by the increase in the green component in the S-nanostructures (Figure 10b,c); the brightness improves with the increase in QY. Figure 10d describes the switchable blue-green emissions in the CIE 1931 chromaticity diagram. The CIE coordinates of blue emission can shift from (0.17, 0.15) to (0.19, 0.25) and the green one from (0.24, 0.35) to (0.26, 0.52) as a function of the PEG-400 amount.

The experimental data show that using a linear polymer, such as PEG-400, in the synthesis of S nanostructures, it is possible to switch their emission from blue to green. The samples obtained only from PEG-400 emit in the blue, excluding the formation of carbonized dots or organic fluorophores that could be responsible for the green emission. At the same time, the emission changes exhibited by the S nanostructures as a function of PEG-400 concentration suggest the presence of direct interactions between the polymer and the S nanosurface. The data from XPS, Raman, and FTIR show that a direct covalent bond forms between the carbon of the PEG-400 and the sulfur of the nanostructures. Furthermore, the polymer modulates the oxidation state of the sulfur atoms at the dot surface and, therefore, the emission. The variations in the S sample emissions when placed in chemical environments with a different degree of polarity and pH indicate that the surface plays a crucial role in modulating the emission. Excitation-independent S nanostructures cannot be defined as quantum dots. In fact, the emission does not depend on the particle size, while a size-dependent emission is the typical signature of quantum confinement. The emission in the present case is due to the surface states. PEG-400 modulates the emission, not just acting as a passivating agent, generally used only to prevent particle aggregation. The linear polymer bonds with the S surface and changes the surface chemical composition that, in turn, controls the emission. Polymers such as PEG-400 are generally defined in nanochemistry as "passivating agents."[10] However, this definition may hide the true nature of the interaction between the polymers and the dot surface.

In most cases, a core-surface model is used to explain the origin of fluorescence in nanodots. This model works quite well, even if precise control of the surface states characterized by the presence of different chemical species is difficult to achieve. In the present case, the experimental results point out that the surface could even play a major role in the emission, and modulation of their chemical composition could be achieved by using polymers, which should be more properly defined as surface modifiers than surface passivators.

CONCLUSIONS

The present work has allowed us to get a better insight into the origin of fluorescence in S nanostructures. Two-color emissive sulfur-based nanostructures have been produced by a sonication-assisted thermal etching of S powders in a strongly basic solution. The addition in the synthesis of a polymer, PEG-400, modulates the optical properties producing different oxidation states of the S atoms at the dot surface. The dimension of the nanoparticles does not change if different amounts of PEG-400 are employed, but the emission switches from blue to green. PEG-400 partially reacts with the sulfide formed from the elemental sulfur dismutation, forming sulfonates and thioethers. The C−S bonds promote the formation of sulfur compounds with a higher degree of oxidation, such as thiosulfate, with respect to the naked S-nanostructures. The peculiar reactivity of PEG-400 allows designing S-nanostructures with controlled blue or green emissions by adjusting the concentration of the passivating agent. The sample emission shifts from blue to green with the increase in the polymer concentration in the solution.

Comprehensive control over the blue-to-green switchable emission should upgrade the S nanomaterials from "promising nanomaterial" status to an innovative tool for advanced devices in optoelectronics and biotechnology.

EXPERIMENTAL SECTION

Chemicals. Sulfur powder (reagent grade, 100 mesh particle size, Sigma-Aldrich), sodium hydroxide (NaOH, 96%, Carlo Erba), sodium deuteroxide (NaOD, D, 99.5%, 30% in D_2O, Cambridge Isotope Laboratories), deuterium oxide (99 atom % D, Sigma-Aldrich), and polyethylene glycol 400 (PEG-400, Alfa Aesar) were used as received without further treatment. Milli-Q water was used for all the experiments.

Synthesis of Bare Sulfur Nanostructures. Sulfur powder (1.4 g) and sodium hydroxide (4.0 g) were added to Milli-Q water (50 mL) and sealed in a glass bottle (capacity of 100 mL). The mixtures in the bottle were sonicated for 7 h in a water bath at 70 °C, in which the suspended mixtures gradually turned into a transparent solution. Then, the solution was purified using a dialysis membrane (2000 MWCO, Sigma-Aldrich) against water for 3 days. Finally, an aqueous solution of bare S dots was obtained by filtering through a 0.22 μm nylon membrane. The dried S nanostructures were collected after evaporating the water in an oven at 60 °C in air.

Synthesis of PEG-Modified Sulfur Nanostructures. At the beginning of the synthesis, a controlled amount of PEG-400 (1.5, 3.0, or 4.5 g) was added to Milli-Q water (50 mL) together with the sulfur powder (1.4 g) and sodium hydroxide (4.0 g). The other synthesis steps were similar to those employed for the synthesis of bare S sample.

Synthesis of PEG Dots. At the beginning of synthesis, PEG-400 (3.0 g) and sodium hydroxide (4.0 g) were added to Milli-Q water (50 mL). The other synthesis steps were similar to those employed for the synthesis of bare S nanostructures.

Synthesis of PEG-Modified Sulfur Nanostructures in the Deuterated Solvent. Sulfur powder (0.567 g) and PEG-400 (1.294 g) were weighted in a 50 mL borosilicate bottle. 14.48 g of D_2O and 4.90 mL of NaOD (30% in D_2O) were then added, and the bottle was sealed with a suba-seal septum. The reaction mixture was then immersed in a water bath preheated at 70 °C and kept under sonication for the whole reaction time. The reaction progress was monitored by sampling 5 mL of the reaction mixture, with a syringe

https://doi.org/10.1021/acs.chemmater.2c02284
Chem. Mater. 2022, 34, 8456−8468

through the suba-seal, after 1, 3, 7, and 13 h of the reaction. The 5 mL of the sample were filtered through polyvinylidene fluoride filters of 0.22 μm, and 500 μL of the resulting clear mixture was analyzed by ^{1}H NMR after diluting them with 500 μL of D_2O containing trimethylsilylpropanoic acid (TMSP).

Characterizations. TEM images were acquired using an FEI Tecnai 200 microscope (Thermo Fisher Scientific) with a field emission gun operating at 200 kV.

XRD patterns of thin films were collected in grazing-incidence geometry using a Bruker D8 Discover diffractometer under irradiation with a Cu Kα_1 line (= 1.54056 Å); the X-ray generator worked at a power of 40 kV and 40 mA. The patterns were recorded in 2θ, ranging from 10 to 70° with a step size of 0.02 Å.

Raman measurements were performed using a "Senterra" Raman microscope (Bruker) under a laser excitation of 532 nm (1 mW power). The spectra were collected with a resolution of ∼3−5 cm^{-1} and an integration time of 10 s.

FTIR spectroscopy analysis was carried out with an "infrared Vertex 70v" interferometer (Bruker) in the absorption mode using a KBr pellet (IR 99%, Sigma). The spectrum of PEG-400 (liquid) was obtained by attenuated total reflection attachment (A225/Q Platinum, Bruker). The baselines were determined by a concave rubber band correction with OPUS 7.0 software.

XPS was carried out in a custom-designed ultrahigh-vacuum (UHV) system equipped with an EA 125 Omicron electron analyzer with five Channeltron, working at a base pressure of 10^{-10} mbar. Core level photoemission spectra were collected in normal emission at room temperature with a non-monochromatized Al Kα X-ray source (1486.7 eV) and using 0.1 eV steps, 0.5 s collection time, and 20 eV pass energy. The S 2p peak has the closely spaced spin−orbit components (S 2p$_{3/2}$ and S 2p$_{1/2}$, Δ = 1.18 eV, branching ratio = 2), which has been set as the standard for the process fitting of the high-resolution spectra. The spectra were fitted by symmetric Voigt functions using a Shirley-type background; the same fit parameters, including the fwhm and Lorentzian−Gaussian ratio, were used for the identical spectral regions.

UV−vis absorption spectroscopy was measured using a Nicolet Evolution 300 UV−vis spectrophotometer (Thermo Fisher) with a bandwidth of 1.5 nm.

Fluorescence spectra were recorded using a "NanoLog" spectrofluorometer (Horiba Jobin Yvon) with a 450 W Xenon lamp for bright UV−vis excitation. The emissive spectra in the visible region were collected by a single-channel detector with 1200-grooves/mm grating. Based on FluorEssence Software, both emission and excitation correction factors were considered to eliminate response characteristics.

The "NanoLog" spectrofluorometer was also used to measure the fluorescence lifetime (TRES) with NanoLED-340 and NanoLED-400 as excitation light sources, respectively; the obtained curves were fitted by DAS6 v6.5 Software.

All NMR spectra were acquired using a Bruker Advance instrument at 600 MHz proton frequency (Bruker BioSpin GmbH, Karlsruhe, Germany). Bruker BBI 5 mm probe with z-gradients was used. All measurements were performed at T = 298 K (Bruker BVT3000 and BCU05 temperature control units). 500 μL of the reaction mixture was diluted with 500 μL of D_2O containing TMSP used as a chemical shift standard (δ = 0 ppm). The spectra were analyzed using MestReNova 14 and OriginPro software.

QY Measurements. The QYs have been evaluated by a relative method according to the following equation

$$\phi = \phi' \times \frac{A'}{I'} \times \frac{I}{A} \times \frac{n^2}{n'^2}$$

where ϕ is the QY of the testing sample, I is the emissive intensity via integration of the testing sample, n is the refractive index of the solvent (1.33 for water), and A is the absorption density at the exciting wavelength. The superscript "′" refers to the corresponding parameters of the dyes as the standard references. Especially, quinine (QY = 55% in 0.1 M H_2SO_4) has been selected as the reference for the emission in the visible range (370−600 nm in this work).

■ ASSOCIATED CONTENT

Supporting Information

The Supporting Information is available free of charge at https://pubs.acs.org/doi/10.1021/acs.chemmater.2c02284.

UV−vis absorption and PL spectra of PEG dots; full UV−vis absorption spectra and calculated QYs of samples; TRES and more PL spectra of bare and PEG-modified S nanostructures; more FTIR of samples; XPS survey spectra of samples; and full-range ^{1}H NMR spectrum of PEG-modified S nanostructures (PDF)

■ AUTHOR INFORMATION

Corresponding Author

Plinio Innocenzi − *Laboratory of Materials Science and Nanotechnology (LMNT), Department of Biomedical Sciences, CR-INSTM, University of Sassari, Sassari 07100, Italy; Department of Chemistry, United Arab Emirates University, Al Ain 15551, United Arab Emirates;* orcid.org/0000-0003-2300-4680; Email: plinio@uniss.it

Authors

Junkai Ren − *Department of Chemical, Physical, Mathematical and Natural Sciences, University of Sassari, Sassari 07100, Italy;* orcid.org/0000-0002-5099-8345

Luca Malfatti − *Laboratory of Materials Science and Nanotechnology (LMNT), Department of Biomedical Sciences, CR-INSTM, University of Sassari, Sassari 07100, Italy;* orcid.org/0000-0001-6901-8506

Luigi Stagi − *Department of Chemical, Physical, Mathematical and Natural Sciences, University of Sassari, Sassari 07100, Italy;* orcid.org/0000-0002-7238-8425

Davide Carboni − *Laboratory of Materials Science and Nanotechnology (LMNT), Department of Biomedical Sciences, CR-INSTM, University of Sassari, Sassari 07100, Italy;* orcid.org/0000-0003-2499-4567

Roberto Anedda − *Porto Conte Ricerche, Alghero SS 07041, Italy;* orcid.org/0000-0003-1235-5821

Laura Calvillo − *Department of Chemical Sciences, University of Padua, Padova 35131, Italy;* orcid.org/0000-0001-9256-0133

Complete contact information is available at: https://pubs.acs.org/10.1021/acs.chemmater.2c02284

Author Contributions

J.R., L.M., and P.I. conceived the study and designed the experiments. J.R., D.C., and L.M. synthesized the materials and performed the characterizations. D.C. and R.A. measured and analyzed the NMR experiments. L.C.L. conducted the XPS measurements and analyzed the data. P.I. supervised the study. J.R., L.M., L.S., D.C., and P.I. wrote and revised the article with contributions from all the authors. All the authors have approved the final version of the manuscript.

Notes

The authors declare no competing financial interest.

■ ACKNOWLEDGMENTS

This work was funded by the Italian Ministry of University and Research (MUR) through project PRIN2017 "CANDL2", grant number 2017W75RAE, and by "Bando competitivo

Fondazione di Sardegna—2017 per progetti di ricerca con revisione tra pari", Progetto MADMAT. Sebastiano Garroni and Matteo Poddighe are gratefully acknowledged for experimental support.

REFERENCES

(1) Yuan, F.; Wang, Y.-K.; Sharma, G.; Dong, Y.; Zheng, X.; Li, P.; Johnston, A.; Bappi, G.; Fan, J. Z.; Kung, H.; Chen, B.; Saidaminov, M. I.; Singh, K.; Voznyy, O.; Bakr, O. M.; Lu, Z.-H.; Sargent, E. H. Bright High-Colour-Purity Deep-Blue Carbon Dot Light-Emitting Diodes via Efficient Edge Amination. *Nat. Photonics* **2020**, *14*, 171−176.

(2) Ren, J.; Stagi, L.; Innocenzi, P. Fluorescent Carbon Dots in Solid-State: From Nanostructures to Functional Devices. *Prog. Solid State Chem.* **2021**, *62*, 100295.

(3) Montalti, M.; Cantelli, A.; Battistelli, G. Nanodiamonds and Silicon Quantum Dots: Ultrastable and Biocompatible Luminescent Nanoprobes for Long-Term Bioimaging. *Chem. Soc. Rev.* **2015**, *44*, 4853−4921.

(4) Gui, R.; Jin, H.; Wang, Z.; Li, J. Black Phosphorus Quantum Dots: Synthesis, Properties, Functionalized Modification and Applications. *Chem. Soc. Rev.* **2018**, *47*, 6795−6823.

(5) Zhu, S.; Song, Y.; Wang, J.; Wan, H.; Zhang, Y.; Ning, Y.; Yang, B. Photoluminescence Mechanism in Graphene Quantum Dots: Quantum Confinement Effect and Surface/Edge State. *Nano Today* **2017**, *13*, 10−14.

(6) Giansante, C.; Infante, I. Surface Traps in Colloidal Quantum Dots: A Combined Experimental and Theoretical Perspective. *J. Phys. Chem. Lett.* **2017**, *8*, 5209−5215.

(7) Ren, J.; Stagi, L.; Malfatti, L.; Carbonaro, C. M.; Granozzi, G.; Calvillo, L.; Garroni, S.; Enzo, S.; Innocenzi, P. Engineering UV-Emitting Defects in h-BN Nanodots by a Top-Down Route. *Appl. Surf. Sci.* **2021**, *567*, 150727.

(8) Li, S.; Chen, D.; Zheng, F.; Zhou, H.; Jiang, S.; Wu, Y. Water-Soluble and Lowly Toxic Sulphur Quantum Dots. *Adv. Funct. Mater.* **2014**, *24*, 7133−7138.

(9) Shen, L.; Wang, H.; Liu, S.; Bai, Z.; Zhang, S.; Zhang, X.; Zhang, C. Assembling of Sulfur Quantum Dots in Fission of Sublimed Sulfur. *J. Am. Chem. Soc.* **2018**, *140*, 7878−7884.

(10) Arshad, F.; Sk, M. P. Luminescent Sulfur Quantum Dots for Colorimetric Discrimination of Multiple Metal Ions. *ACS Appl. Nano Mater.* **2020**, *3*, 3044−3049.

(11) Wang, H.; Wang, Z.; Xiong, Y.; Kershaw, S. V.; Li, T.; Wang, Y.; Zhai, Y.; Rogach, A. L. Hydrogen Peroxide Assisted Synthesis of Highly Luminescent Sulfur Quantum Dots. *Angew. Chem., Int. Ed.* **2019**, *58*, 7040−7044.

(12) Song, Y.; Tan, J.; Wang, G.; Gao, P.; Lei, J.; Zhou, L. Oxygen Accelerated Scalable Synthesis of Highly Fluorescent Sulfur Quantum Dots. *Chem. Sci.* **2020**, *11*, 772−777.

(13) Wang, Y.; Zhao, Y.; Wu, J.; Li, M.; Tan, J.; Fu, W.; Tang, H.; Zhang, P. Negatively Charged Sulfur Quantum Dots for Treatment of Drug-Resistant Pathogenic Bacterial Infections. *Nano Lett.* **2021**, *21*, 9433−9441.

(14) Sheng, Y.; Huang, Z.; Zhong, Q.; Deng, H.; Lai, M.; Yang, Y.; Chen, W.; Xia, X.; Peng, H. Size-Focusing Results in Highly Photoluminescent Sulfur Quantum Dots with a Stable Emission Wavelength. *Nanoscale* **2021**, *13*, 2519−2526.

(15) Zhang, C.; Zhang, P.; Ji, X.; Wang, H.; Kuang, H.; Cao, W.; Pan, M.; Shi, Y.; Wang, Z. Ultrasonication-Promoted Synthesis of Luminescent Sulfur Nano-Dots for Cellular Imaging Applications. *Chem. Commun.* **2019**, *55*, 13004−13007.

(16) Gao, P.; Wang, G.; Zhou, L. Luminescent Sulfur Quantum Dots: Synthesis, Properties and Potential Applications. *ChemPhotoChem* **2020**, *4*, 5235−5244.

(17) Jin, H.; Sun, Y.; Sun, Z.; Yang, M.; Gui, R. Zero-Dimensional Sulfur Nanomaterials: Synthesis, Modifications and Applications. *Coord. Chem. Rev.* **2021**, *438*, 213913.

(18) Ning, K.; Sun, Y.; Liu, J.; Fu, Y.; Ye, K.; Liang, J.; Wu, Y. Research Update of Emergent Sulfur Quantum Dots in Synthesis and Sensing/Bioimaging Applications. *Molecules* **2022**, *27*, 2822.

(19) Manan, N. S. A.; Aldous, L.; Alias, Y.; Murray, P.; Yellowlees, L. J.; Lagunas, M. C.; Hardacre, C. Electrochemistry of Sulfur and Polysulfides in Ionic Liquids. *J. Phys. Chem. B* **2011**, *115*, 13873−13879.

(20) Ren, J.; Malfatti, L.; Enzo, S.; Carbonaro, C. M.; Calvillo, L.; Granozzi, G.; Innocenzi, P. Boron Oxynitride Two-Colour Fluorescent Dots and their Incorporation in a Hybrid Organic-Inorganic Film. *J. Colloid Interface Sci.* **2020**, *560*, 398−406.

(21) Vonk, S. J. W.; Fridriksson, M. B.; Hinterding, S. O. M.; Mangnus, M. J. J.; van Swieten, T. P.; Grozema, F. C.; Rabouw, F. T.; van der Stam, W. Trapping and Detrapping in Colloidal Perovskite Nanoplatelets: Elucidation and Prevention of Nonradiative Processes through Chemical Treatment. *J. Phys. Chem. C* **2020**, *124*, 8047−8054.

(22) Arshad, F.; Sk, M. P.; Maurya, S. K.; Siddique, H. R. Mechanochemical Synthesis of Sulfur Quantum Dots for Cellular Imaging. *ACS Appl. Nano Mater.* **2021**, *4*, 3339−3344.

(23) Xiao, L.; Du, Q.; Huang, Y.; Wang, L.; Cheng, S.; Wang, Z.; Wong, T. N.; Yeow, E. K. L.; Sun, H. Rapid Synthesis of Sulfur Nanodots by One-Step Hydrothermal Reaction for Luminescence-Based Applications. *ACS Appl. Nano Mater.* **2019**, *2*, 6622−6628.

(24) Eichinger, I.; Schmitz-Esser, S.; Schmid, M.; Fisher, C. R.; Bright, M. Symbiont-Driven Sulfur Crystal Formation in a Thiotrophic Symbiosis from Deep-Sea Hydrocarbon Seeps. *Environ. Microbiol. Rep.* **2014**, *6*, 364−372.

(25) Jeffrey, M. I.; Watling, K.; Hope, G. A.; Woods, R. Identification of Surface Species that Inhibit and Passivate Thiosulfate Leaching of Gold. *Miner. Eng.* **2008**, *21*, 443−452.

(26) Socrates, G. *Infrared and Raman Characteristic Group Frequencies: Tables and Charts*, 3rd ed.; John Wiley & Sons: Middlesex, 2001; pp 125−129.

(27) Teja-Ruiz, A. M.; Juárez-Tapia, J. C.; Hernández-Cruz, L. E.; Reyes-Pérez, M.; Patiño-Cardona, F.; Reyes-Dominguez, I. A.; Flores-Guerrero, M. U.; Palacios-Beas, E. G. Influence of Temperature on the Formation of Ag Complexed in a S2O32−-O2 System. *Minerals* **2017**, *7*, 16.

(28) Alemdar, A.; Güngör, N.; Ece, O. I.; Atici, O. The Rheological Properties and Characterization of Bentonite Dispersions in the Presence of Non-Ionic Polymer PEG. *J. Mater. Sci.* **2005**, *40*, 171−177.

(29) Ren, J.; Stagi, L.; Malfatti, L.; Garroni, S.; Enzo, S.; Innocenzi, P. Boron Nitride−Titania Mesoporous Film Heterostructures. *Langmuir* **2021**, *37*, 5348−5355.

(30) Ren, J.; Stagi, L.; Carbonaro, C. M.; Malfatti, L.; Casula, M. F.; Ricci, P. C.; Del Rio Castillo, A. E.; Bonaccorso, F.; Calvillo, L.; Granozzi, G.; Innocenzi, P. Defect-Assisted Photoluminescence in Hexagonal Boron Nitride Nanosheets. *2D Mater.* **2020**, *7*, 045023.

(31) Liu, S.; Wang, H.; Feng, A.; Chang, J.; Zhang, C.; Shi, Y.; Zhai, Y.; Biju, V.; Wang, Z. Photoluminescence Investigations of Sulfur Quantum Dots Synthesized by a Bubbling-Assisted Strategy. *Nanoscale Adv.* **2021**, *3*, 4271−4275.

(32) Lin, Y.-C.; Chen, Y.-Y.; Yu, B.-Y.; Lin, W.-C.; Kuo, C.-H.; Shyue, J.-J. Sputter-Induced Chemical Transformation in Oxoanions By Combination of $C60^+$ and Ar^+ Ion Beams Analyzed with X-Ray Photoelectron Spectrometry. *Analyst* **2009**, *134*, 945−951.

(33) Chu, H.; Noh, H.; Kim, Y.-J.; Yuk, S.; Lee, J.-H.; Lee, J.; Kwack, H.; Kim, Y.; Yang, D.-K.; Kim, H.-T. Achieving Three-Dimensional Lithium Sulfide Growth in Lithium-Sulfur Batteries Using High-Donor-Number Anions. *Nat. Commun.* **2019**, *10*, 188.

(34) Shanthi, P. M.; Hanumantha, P. J.; Ramalinga, K.; Gattu, B.; Datta, M. K.; Kumta, P. N. Sulfonic Acid Based Complex Framework Materials (CFM): Nanostructured Polysulfide Immobilization Systems for Rechargeable Lithium−Sulfur Battery. *J. Electrochem. Soc.* **2019**, *166*, A1827−A1835.

(35) Razzaq, A. A.; Yao, Y.; Shah, R.; Qi, P.; Miao, L.; Chen, M.; Zhao, X.; Peng, Y.; Deng, Z. High-Performance Lithium Sulfur

https://doi.org/10.1021/acs.chemmater.2c02284
Chem. Mater. 2022, 34, 8456−8468

Batteries Enabled by a Synergy between Sulfur and Carbon Nanotubes. *Energy Storage Mater.* **2019**, *16*, 194−202.
(36) Mahou, R.; Wandrey, C. Versatile Route to Synthesize Heterobifunctional Poly(ethylene glycol) of Variable Functionality for Subsequent Pegylation. *Polymers* **2012**, *4*, 561−589.
(37) Yu, L.; Zheng, Z.; Liu, Y.; Li, Z.; Wang, X. Synthesis and Properties of Tunable Thermoresponsive Aliphatic Polycarbonate Copolymers with Oligo Ethylene Glycol Containing Thioether and/or Sulphone Groups. *RSC Adv.* **2015**, *5*, 64832−64840.
(38) Solvent and Environmental Effects. *Principles of Fluorescence Spectroscopy*; Lakowicz, J. R., Ed.; Springer US: Boston, MA, 2006; pp 205−235.
(39) Zhang, T.; Zhu, J.; Zhai, Y.; Wang, H.; Bai, X.; Dong, B.; Wang, H.; Song, H. A Novel Mechanism for Red Emission Carbon Dots: Hydrogen Bond Dominated Molecular States Emission. *Nanoscale* **2017**, *9*, 13042−13051.
(40) Ren, J.; Sun, J.; Sun, X.; Song, R.; Xie, Z.; Zhou, S. Precisely Controlled Up/Down-Conversion Liquid and Solid State Photoluminescence of Carbon Dots. *Adv. Opt. Mater.* **2018**, *6*, 1800115.
(41) Snyder, L. R. Classification off the Solvent Properties of Common Liquids. *J. Chromatogr.* **1978**, *16*, 223−234.
(42) Zhu, S.; Meng, Q.; Wang, L.; Zhang, J.; Song, Y.; Jin, H.; Zhang, K.; Sun, H.; Wang, H.; Yang, B. Highly Photoluminescent Carbon Dots for Multicolor Patterning, Sensors, and Bioimaging. *Angew. Chem., Int. Ed.* **2013**, *52*, 3953−3957.

https://doi.org/10.1021/acs.chemmater.2c02284
Chem. Mater. 2022, 34, 8456−8468